Sensors & Actuators: B. Chemical 307 (2020) 127619

Contents lists available at ScienceDirect

Sensors and Actuators B: Chemical

journal homepage: www.elsevier.com/locate/snb

Highly-sensitive electrochemiluminescence biosensor for NT-proBNP using MoS_2@Cu_2S as signal-enhancer and multinary nanocrystals loaded in mesoporous UiO-66-NH_2 as novel luminophore

Chao Wang[a], Lei Liu[a], Xuejing Liu[a], Yu Chen[a], Xueying Wang[a], Dawei Fan[a], Xuan Kuang[a], Xu Sun[a], Qin Wei[a,*], Huangxian Ju[a,b,*]

[a] Collaborative Innovation Center for Green Chemical Manufacturing and Accurate Detection, Key Laboratory of Interfacial Reaction & Sensing Analysis in Universities of Shandong, School of Chemistry and Chemical Engineering, University of Jinan, Jinan 250022, PR China
[b] State Key Laboratory of Analytical Chemistry for Life Science, College of Chemistry and Chemical Engineering, Nanjing University, Nanjing 210023, PR China

ARTICLE INFO

Keywords:
Electrochemiluminescence
Nanocrystal
Coreaction accelerator
NT-proBNP
Mesoporous MOF
Immunosensor

ABSTRACT

The accurate clinical diagnosis and prognosis keep ultrasensitive detection of NT-proBNP in a necessary topic. This work proposes a "signal-on" electrochemiluminescence (ECL) biosensor for ultrasensitive quantification of NT-proBNP with a newly designed luminophore. The luminophore is prepared by depositing Mn-doped ZnAgInS/ZnS nanocrystals in thermally-treated UiO-66-NH_2 with mesoporous cages. Appropriate Mn doping enhances the stable luminescence, and the presence of ZnS shell reduces the surface defects to boost the quantum yield. The immunosensor is prepared by immobilizing the capture antibody on Au nanoparticles loaded MoS_2@Cu_2S modified electrode. The MoS_2@Cu_2S composite is synthesized by depositing MoS_2 nanosheets on Cu_2S snowflake, which forms distinct ripples on snowflake-like architecture to endow MoS_2@Cu_2S with considerable catalytic active sites as coreaction accelerator for amplifying the ECL signal. By labeling the detection antibody with the novel luminophore, a sandwich immunoassay is developed for ECL detection of NT-proBNP with a linear scope of 1 fg mL^{-1}–100 ng mL^{-1} and a detection limit of 0.41 fg mL^{-1}. Considering the excellent stability and selectivity, this paper exploits an innovative way to synthesize MOFs based luminophores and offers a powerful and responsible method for clinical assessment of biomarkers.

1. Introduction

Heart failure (HF) is a burgeoning health issue as its death risk is comparable to some cancers. It is a common problem among the elderly on account of cardiovascular disease. Moreover, it can happen at any age, even in fetus [1]. As a newly developed biomarker of HF, amino-terminal pro-brain natriuretic peptides (NT-proBNP) is better than BNP for its longer half-life period and higher stability in vitro [2]. The age-classified thresholds of serum NT-proBNP level are listed as follows: (1) > 1.8 ng mL^{-1} for patients older than 75 years old, (2) > 900 pg mL^{-1} for patients aged between 50 and 75 years old, (3) > 450 pg mL^{-1} for patients younger than 50 years old [3]. Hence, the sensitive and specific evaluation of NT-proBNP level holds tremendous significance in reducing the mortality and expenditure related with HF. Up to now, several analytical techniques, such as surface plasma resonance [4], electrochemical [5], chemiluminescence [6] and photochemical [7] methods, have been employed to quantify NT-proBNP. Besides these techniques, electrochemiluminescence (ECL) has also been used as a powerful tool for bioassay [8,9] due to the high sensitivity and simplicity of electrochemical method and the merits of low background noise and wide detection range inherited from chemiluminescence.

Since Ju and Zou proposed the ECL biosensing of nanocaystals (NCs) [10], III–V and II–IV group NCs have been extensively explored in ECL field owing to their size/composition-dependent ECL property and easy of surface modification [11,12]. Considering the intrinsic toxicity of Cd in bioassay application of these NCs, eco-friendly I–III–IV NCs might provide a promising alternative to traditional binary NCs [13]. As an outstanding representative of I–III–IV NCs, ZnAgInS has exerted a tremendous fascination on bio-labeling and bio-imaging thanks to its adjustable band gap, desirable optoelectronic properties and fine biocompatibility [14,15]. Furthermore, soon after the innovative research of Mn-doped ZnS in 1994 [16], enormous endeavors have been paid to

* Corresponding authors at: Collaborative Innovation Center for Green Chemical Manufacturing and Accurate Detection, Key Laboratory of Interfacial Reaction & Sensing Analysis in Universities of Shandong, School of Chemistry and Chemical Engineering, University of Jinan, Jinan 250022, PR China.
E-mail addresses: sdjndxwq@163.com (Q. Wei), hxju@nju.edu.cn (H. Ju).

https://doi.org/10.1016/j.snb.2019.127619
Received 6 November 2019; Received in revised form 30 November 2019; Accepted 21 December 2019
Available online 24 December 2019
0925-4005/

explore Mn doped NCs as the forefront of luminescent materials for the reasons that Mn doping can enhance the photoluminescence to achieve strong and stable emission and alleviate the emission of self-absorption with large Stokes shift [17–19]. Encouraged by these praisable properties, this work synthesized Mn doped ZnAgInS (MZnAgInS) via facile homogenous nucleation doping method. However, the rapid nucleation and growth process produced many defects and free linkages on the surface of MZnAgInS NCs, which declined the quantum yield. Fortunately, this phenomenon could be avoided tactfully by coating another semiconductor material with wide band gap on its surface. Herein, ZnS, which has bulk band gap (E_g = 3.7 eV) and little lattice mismatch with MZnAgInS, was chosen as the coating layer to reduce the surface defects and enhance the quantum yield and emission stability [20]. To the best of our knowledge, it was the first time to employ MZnAgInS/ZnS NC as the electrochemiluminophore for biosensing application.

Recently, nanomaterial-based signal amplification has become a prevalent strategy to boost the sensitivity of biosensing because the large specific surface area and easy surface modification are conducive to immobilize more signal probes. UiO-66-NH_2 (UiO for University of Oslo), as a classic series of Zr-based metal-organic framework (MOF) with intriguing aesthetic structure and high structural stability [21], is expected to serve as stabilizing matrix for loading more MZnAgInS/ZnS NCs. However, the pore diameter of UiO-66-NH_2 is merely 0.8 nm [22], which limits the incorporation of MZnAgInS/ZnS NC. By tuning the organic ligands and metal center at molecular level, the chemical structure of UiO-66-NH_2 can be modified flexibly [23,24]. In this protocol, the pore size of UiO-66-NH_2 was firstly enlarged by thermally treating at 300 °C to remove a part of organic functionalities. The resulted UiO-66-NH_2 (denoted as t-UiO-66-NH_2) with mesoporous cages could not only serve as the anchor carrier for the enrichment of NCs, but also alleviate the inner filter effect efficaciously for the enhancement of ECL emission. The newly designed luminophore could be conveniently labeled to the detection antibody (Ab_2) for design of ECL immunoassay (Scheme 1A).

To achieve highly sensitive ECL immunoassay, another signal amplification strategy was achieved on the immunosensor by employing nanomaterial with excellent catalytic performance as coreaction accelerator to speed up the electrochemical reaction for generation of more active intermediates [25,26]. This strategy has been reported by using MoS_2 nanoflower [27], flowerlike MoS_2/GO/MWCNT [13], CuS nanoparticles [28], and CuS porous nanospheres [29] as the co-reaction accelerator. This work deposited MoS_2 nanosheets on Cu_2S snowflake to obtain the coreaction accelerator MoS_2@Cu_2S with considerable catalytic active sites, and then loaded Au NPs for preparation of immunosensor (Scheme 1B). The snowflake-like MoS_2@Cu_2S-Au architecture possessed large specific surface area for loading of capture antibody (Ab_1), and effective catalytic performance and high conductivity for accelerating the ECL reaction. Thus, a "signal-on" ECL immunosensor with a detection range of 8 orders of magnitude was constructed for NT-proBNP.

2. Experimental section

2.1. Synthesis of MoS_2@Cu_2S-Au composite

MoS_2@Cu_2S composite was prepared according previous report with little modification [30]. The Cu_2S snowflakes were synthesized via hydrothermal method. 0.1705 g of $CuCl_2{\cdot}2H_2O$ was dissolved in 30 mL of ethylenediamine by ultrasound. Then, 0.2284 g of thiourea was added to this ianthinus suspension and stirred for 2 h. The resulted solution was moved to a 50 mL of Teflon-lined stainless-steel autoclave and heated at 80 °C for 8 h. The Cu_2S snowflakes were isolated by centrifugation after cooling down to room temperature and washed thoroughly with ethanol for three times. For the preparation of MoS_2@Cu_2S, 0.02420 g of $Na_2MoO_4{\cdot}2H_2O$ and 0.07612 g of thiourea were dispersed in 20 mL of ultrapure water. 20 mg of Cu_2S was then added and blended for 5 min to form homogeneous solution. After reaction at 200 °C for 24 h, the MoS_2@Cu_2S was obtained. To synthesize MoS_2@Cu_2S-Au, 10 mg of MoS_2@Cu_2S was mixed with 5 mL of Au NPs sol (the preparation process of Au NPs was illustrated in Supplementary materials) and shaken for one day. After centrifugation, MoS_2@Cu_2S-Au composite was dispersed in 5 mL of phosphate buffer saline (PBS, pH 7.5) for further use.

2.2. Synthesis of MZnAgInS/ZnS@t-UiO-66-NH_2-Ab_2

UiO-66-NH_2 was prepared according to the following protocol [31]. Typically, 0.096 g of 2-aminoterephthalic acid, 0.120 g of $ZrCl_4$ and 4 mL of acetic acid were dispersed in 32 mL of dimethyl formamide (DMF) and agitated for 30 min. Afterward, the resultant solution was transferred to a 50 mL of Teflon-lined stainless-steel autoclave and reacted at 120 °C for 24 h. The UiO-66-NH_2 precipitate was collected after centrifugation and immersed into ethanol for 48 h to exchange DMF from the product. To enlarge the pore diameter, UiO-66-NH_2 powder was thermally treated at 300 °C in air for 6 h and then activated at 75 °C

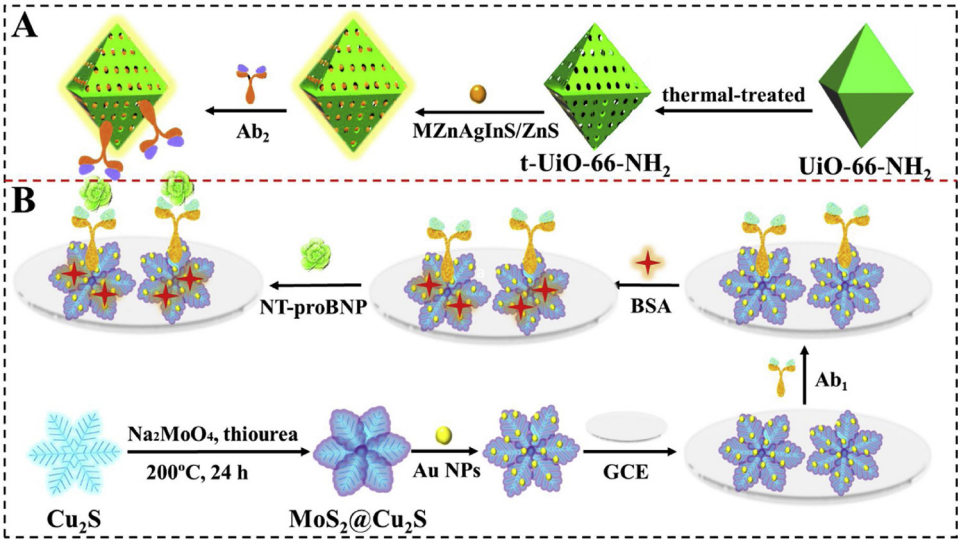

Scheme 1. (A) Preparation of luminophore and Ab_2 bioconjugates. (B) Fabrication of ECL immunosensor and its recognition to NT-proBNP.

under vacuum to remove the residual solvent in the pore. The resulting product was denoted as t-UiO-66-NH_2 for convenience.

The preparation process of MZnAgInS/ZnS NCs was described as follows. For synthesis of MZnAgInS with molar ratio of Mn:Ag as 3:4, 10 mL of ultrapure water containing 0.0085 g of $AgNO_3$, 0.0602 g of In $(NO_3)_3$, 0.0439 g of $Zn(CH_3COO)_2{\cdot}2H_2O$ and 0.00918 g of Mn $(CH_3COO)_2$ was stirred for 5 min, and then 2 mL of L-cysteine (0.6 mol L^{-1}) was added and the pH of the mixture was adjusted to 8.5 using NaOH (6 mol L^{-1}). Finally, 6.5 mL of thioacetamide (0.05 mol L^{-1}) was introduced to the mixture, and the resultant solution was sealed in a Teflon reaction kettle to maintain at 110 °C for 4 h. After centrifugation and washed with ethanol for 3 times, the obtained MZnAgInS was redispersed in 10 mL of ultrapure water. To prepare MZnAgInS/ZnS NCs, 10 mL of MZnAgInS was loaded in a three-neck flask and oil-bathed to 100 °C. After injection of 1 mL of Zn $(CH_3COO)_2{\cdot}2H_2O$ (0.05 mol L^{-1}), the solution was refluxed at 100 °C for 2 h. Be separated by centrifugation, the MZnAgInS/ZnS NCs were scattered in 10 mL of ultrapure water.

To prepare MZnAgInS/ZnS@t-UiO-66-NH_2-Ab_2, 10 mg of t-UiO-66-NH_2 was mixed with 10 mL of MZnAgInS/ZnS and stirred at room temperature for 8 h. Once centrifugation was finished, MZnAgInS/ZnS@t-UiO-66-NH_2 was dispersed in 2 mL of PBS (pH 7.5). Then, 1 mL of 10 μg mL^{-1} NT-proBNP Ab_2, which was activated with 1 mL PBS containing 1-ethyl-3-(3-dimethylaminopropyl) carbodiimide (EDC, 20 mmol) and *N*-hydroxysuccinimide (NHS, 10 mmol), was added to 2 mL of MZnAgInS/ZnS@t-UiO-66-NH_2 solution and oscillated at 4 °C overnight. After centrifugation, the resulting Ab_2 bioconjugate was scattered in 1 mL of PBS (pH 7.5) and kept at 4 °C.

2.3. Fabrication of immunosensor

In the beginning, glassy carbon electrode (GCE) with 4 mm in diameter was polished by using 0.05 and 0.3 μm Al_2O_3 slurry and rinsed completely by using pure water. Next, 6 μL of MoS_2@Cu_2S -Au was dispersed on the GCE surface and dried naturally. Afterwards, 5 μL of Ab_1 (10 μg mL^{-1}) was captured on the GCE surface through Au-NH_2 bond. Succeedingly, the immunosensor was washed meticulously by PBS (pH 7.5) and treated with 3 μL of BSA (1 wt%) to prevent nonspecific adsorption.

2.4. ECL detection of NT-proBNP

6 μL of NT-proBNP with different concentrations (1 fg mL^{-1}–100 ng mL^{-1}) was covered on the immunosensors and incubated at 4 °C for 12 h. Ultimately, the immunosensors were rinsed with PBS (pH 7.5) and reacted with 6 μL of Ab_2 bioconjugate. After the formation of immune-complexes, the unbound Ab_2 were rinsed away with PBS (pH 7.5) to perform ECL detection with model MPI-E ECL analyzer (Remax, China) in 10 mL of PBS (pH 7.5) containing 0.1 M $K_2S_2O_8$ under the potential scan from 0 V to −1.7 V. The voltage of photomultiplier tube was set at 700 V, and the scan rate was fixed at 100 mV s^{-1}.

3. Results and discussion

3.1. Material characterization

The morphology and composition of different materials were characterized by scanning electron microscopy (SEM), transmission electron microscopy (TEM) and X-ray diffraction (XRD). As depicted in Fig. 1A, the snowflake-like Cu_2S exhibited regularly six oriented petals with the length of each dendrite about 6 μm. The partial SEM image of MoS_2@Cu_2S showed innumerably ultrathin MoS_2 nanosheets on the surface of Cu_2S (Fig. 1B). N_2 adsorption-desorption measurements were further implemented to compare the specific surface area of Cu_2S and MoS_2@Cu_2S. The BET specific surface area of Cu_2S and MoS_2@Cu_2S were 18.4 and 21.6 $m^2 g^{-1}$ respectively (Fig. 2A), proving that MoS_2@Cu_2S possessed larger specific surface area than Cu_2S. The distinct ripples on unparalleled snowflake-like architecture endowed the immunosensing platform with large specific surface area to load more capture antibodies and supply more catalytic active sites for coreactant decomposition. It could be observed from the TEM image of MoS_2@Cu_2S-Au (Fig. 1C) that tiny Au NPs were linked with MoS_2@Cu_2S via Au-S bond successfully. The energy dispersive spectrometer (EDS) mapping drawings with distinct color contrast for Cu, Mo and S elements (Fig. 1D) further proved the success of MoS_2@Cu_2S preparation. Besides, XRD of MoS_2@Cu_2S was also matched well with orthorhombic Cu_2S (JCPDS card No.02-1294), and all the intense peaks of MoS_2 in the diagram of MoS_2@Cu_2S were assigned to rhombohedral MoS_2 (JCPDS card No.17-0744) (Fig. 1E).

The SEM image of t-UiO-66-NH_2 confirmed its highly mono-dispersed octahedral morphology with average diameter of 700 nm (Fig. 1F), and such distinct morphology features was also evidenced in TEM (Fig. 1G). The XRD patterns of UIO-66-NH_2 and t-UiO-66-NH_2 showed the characteristic peaks of t-UiO-66-NH_2 similar to that of UiO-66-NH_2 (Fig. 2B), and all the characteristic diffraction peaks were in well conformity to the simulated ones. Besides, no ZrO_2 and other diffraction peaks of impurities was observed, illustrating that the crystallinity of UiO-66-NH_2 was not destroyed after thermal treatment. To investigate the stability of UiO-66-NH_2 at high temperature, thermogravimetric analysis (TGA) was carried out. As shown in Fig. 2C, the structure of UiO-66-NH_2 was destroyed as the temperature elevated to 400 °C. Before the heating temperature reached 400 °C, a fraction of function groups were removed and resulted in the formation of defects in the porous structure. Hence, it was sensible to enlarge the pore size of UiO-66-NH_2 by thermally treatment at 300 °C. Meanwhile, N_2 adsorption-desorption isotherms and related pore size distribution were also investigated to prove the enlargement of pore size for t-UiO-66-NH_2 (Fig. 2D). The t-UiO-66-NH_2 possessed a BET specific surface area about 701 $m^2 g^{-1}$, which was in sharp contrast to the original UiO-66-NH_2 (979 $m^2 g^{-1}$). The decline of surface area further confirmed the enlargement of pore size. The pore size of t-UiO-66-NH_2 was distributed approximately at 3.12 nm (Fig. 2E), which was suitable for the accommodation of MZnAgInS/ZnS NCs. Further examination of MZnAgInS/ZnS morphology and size distribution with TEM (Figs. 1H and 2 F) revealed that MZnAgInS/ZnS NCs were of uniform spherical nanostructure with mean diameter of 1.80 nm. After the incorporation of MZnAgInS/ZnS into t-UiO-66-NH_2, tiny salient points could be observed on the surface of t-UiO-66-NH_2 (Fig. 1I), and the morphology of t-UiO-66-NH_2 was not changed significantly. The EDS mapping, particularly the identification of Mn and Zn, further certified the uniform distribution of MZnAgInS/ZnS on t-UiO-66-NH_2 (Fig. 1I). The EDS of MZnAgInS/ZnS@t-UiO-66- NH_2 showed apparently the major elements such as Zr, C, O, Mn, Zn, Ag, In and S (Fig.1J).

3.2. Electrochemical characterization of the immunosensor

Electrochemical impedance spectroscopy (EIS) was performed to verify the successful assembly steps of this immunosensor (Fig. 3A). The relevant data, which were simulated by ZSimWin software, were listed in Table S1. The diameter of semicircle in the Nyquist plots was related with the electro-transfer resistance (R_{et}) at the electrode/solution interface. The EIS curve of bare GCE (curve a) was almost a straight line. When GCE was modified with MoS_2@Cu_2S-Au, a small semicircle diameter was obtained (curve b), manifesting the favorable conductivity of this immunosensing interface. After the continuous modifications of nonconductive Ab_1, Ag, BSA on the electrode, the resistance increased sequentially (curves c, d and e). The electrode experienced a further resistance enhancement when MZnAgInS/ZnS@t-UiO-66-NH_2-Ab_2 was conjugated with Ag, suggesting the immunoreation occurred between Ag and Ab_2 bioconjugate as expected. To better understand the interfacial characteristics of different modified electrodes, cyclic

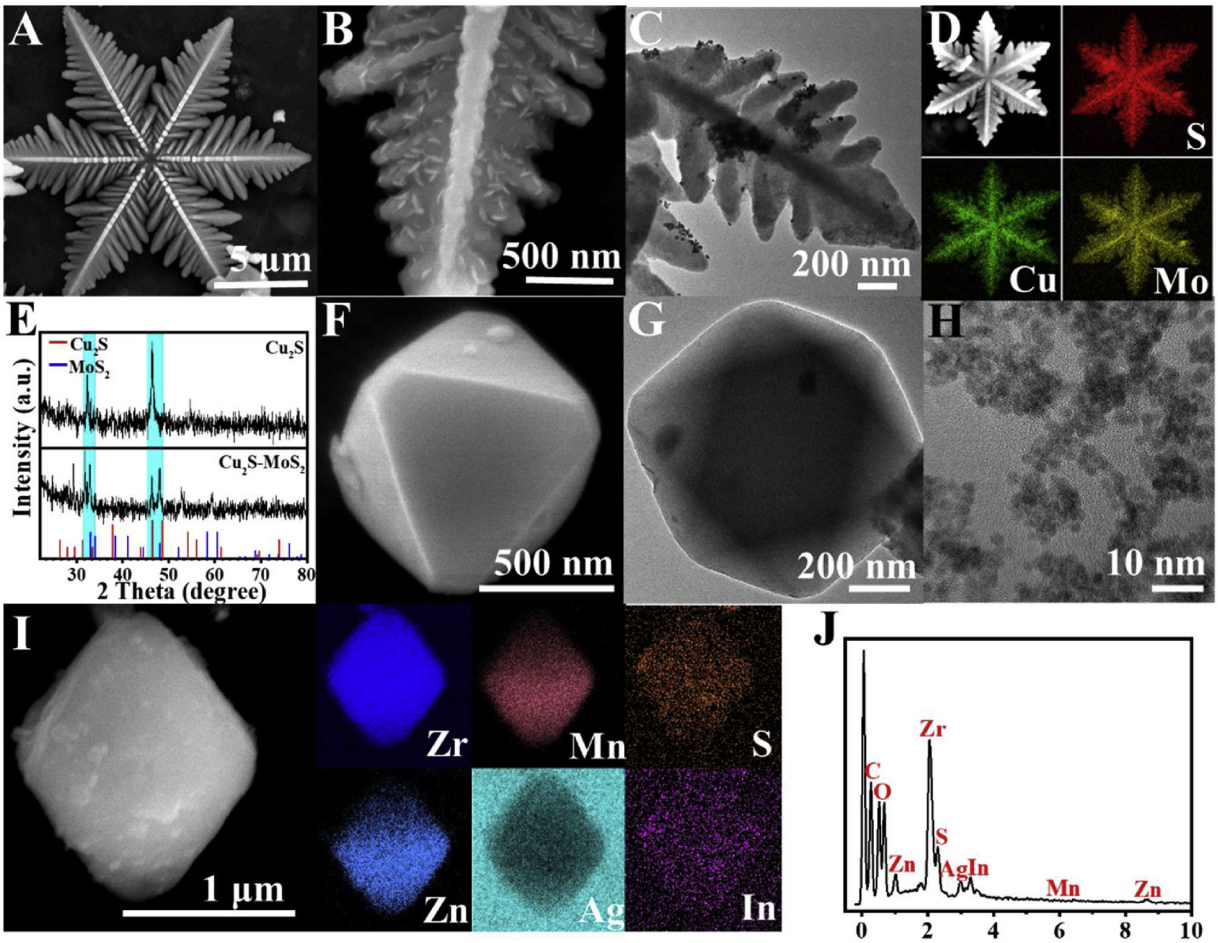

Fig. 1. SEM of (A) Cu_2S and (B) MoS_2@Cu_2S. (C) TEM of MoS_2@Cu_2S-Au. (D) Mapping of MoS_2@Cu_2S. (E) XRD of MoS_2@Cu_2S. (F) SEM and (G) TEM of t-UiO-66-NH_2. (H) TEM of MZnAgInS/ZnS. (I) Mapping and (J) EDS of MZnAgInS/ZnS@t-UiO-66-NH_2.

voltammetry was adopted to characterize the fabrication course. As observed in Fig. 3B, the CV results were well in accordance with the EIS characterization, testifying the success of immunosensor construction.

3.3. ECL signal amplification strategy

Control experiments were conducted to elucidate the ECL signal amplification tactics and the superiority of MZnAgInS/ZnS@t-UiO-66-NH_2 (Fig. 3C). The pristine ZnAgInS NCs exhibited weak ECL signal in the presence of $K_2S_2O_8$ (curve a). After the appropriate dopant of Mn in ZnAgInS NCs, the ECL signal increased (curve b) since the interaction of Mn dopants with ternary host NCs could alleviate the emission of self-absorption with large Stokes shift [32]. The presence of ZnS shell enabled an almost 3.5-fold enhancement of ZnAgInS ECL signal (curve c) because ZnS shell could reduce surface defects and widened the band gap of MznAgInS [33]. The t-UiO-66-NH_2 also played a vital role in the signal amplification of MZnAgInS/ZnS, as evidenced in curve d, the considerable surface area and suitable pore diameter endowed t-UiO-66-NH_2 with the ability to deposit MZnAgInS/ZnS NCs substantially, thus the ECL probe prepared in this protocol exhibited strong and stable ECL emission.

To get a deep insight into the influence of MoS_2@Cu_2S exerted on the ECL behavior of MZnAgInS/ZnS@t-UiO-66-NH_2, the ECL intensity of MZnAgInS/ZnS@t-UiO-66-NH_2 modified electrode was measured by using various solutions as the electrolyte. As observed from curve a and b in Fig. 3D, $K_2S_2O_8$ was an effective coreactant of MZnAgInS/ZnS@t-UiO-66-NH_2. After dropping 500 μL of Cu_2S and MoS_2 solution into 10 mL of PBS (pH 7.5) containing 0.1 M $K_2S_2O_8$ respectively, conspicuous enhancement of ECL responses were obtained. It could be concluded from curve c and d that both Cu_2S and MoS_2 could accelerate the decomposition of $S_2O_8^{2-}$ to generate more $SO_4^{\cdot-}$, thus more excited state of MZnAgInS/ZnS NCs could be produced. As contrast to curve c and d, when MoS_2@Cu_2S was employed as the coreaction accelerator, the ECL response witnessed a remarkable enhancement (curve e), which was comparable to 1.8-time of ECL intensity obtained from MZnAgInS/ZnS@t-UiO-66-NH_2 with merely $K_2S_2O_8$ as the coreatant, confirming the synergic effect of MoS_2 and Cu_2S on catalyzing the reduction of $K_2S_2O_8$. Moreover, the bare electrode with $K_2S_2O_8$ as the electrolyte exhibited negligible ECL emission (curve f) due to the ECL property of singlet oxygen. After the addition of 500 μL of MoS_2@Cu_2S solution, the ECL intensity increased to almost 10-time of its initial value (curve g), proving that MoS_2@Cu_2S was reacted with $K_2S_2O_8$ rather than luminophore to amplify the ECL emission. The electrochemical property of MoS_2@Cu_2S was also explored to elucidate the catalytic mechanism and the details were provided in Supplementary materials (Fig. S1).

The above discussion revealed that Mn dopant and ZnS shelling could improve the ECL performance of ZnAgInS NCs, and t-UiO-66-NH_2 could increase the amount of immobilized MZnAgInS/ZnS, thus the ECL response was enhanced to a large extent. Meanwhile, MoS_2@Cu_2S could act as an effective coreaction accelerator to expedite the generation of strong oxidant $SO_4^{\cdot-}$ for further ECL signal amplification. The possible ECL mechanism was outlined as follows.

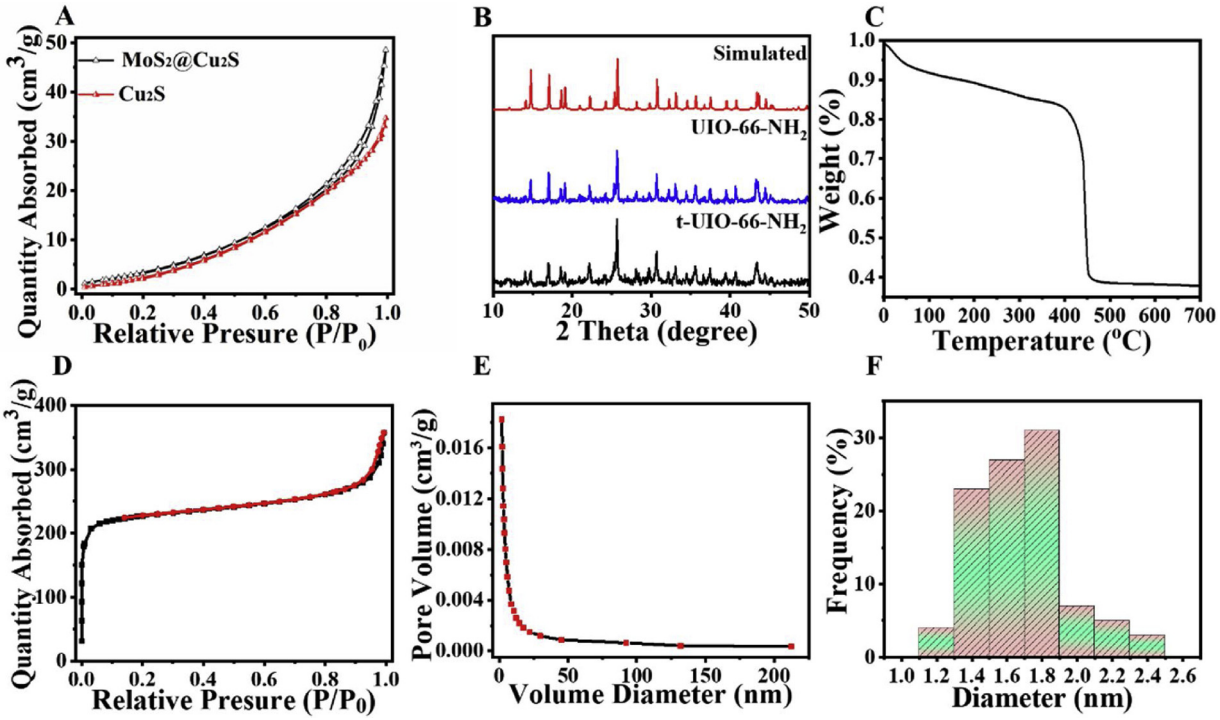

Fig. 2. (A) Nitrogen adsorption-desorption isotherms of Cu_2S (red curve) and MoS_2@Cu_2S (black curve). (B) XRD patterns of UiO-66-NH_2 and t-UiO-66-NH_2. (C) Thermogravimetric analysis (TGA) curve of UiO-66-NH_2. (D) Nitrogen adsorption-desorption isotherms of t-UiO-66-NH_2. (E) Pore size distribution of t-UiO-66-NH_2. (F) Size distribution of MZnAgInS/ZnS nanocrystals. (For interpretation of the references to colour in this figure legend, the reader is referred to the web version of this article.)

3.4. Optimization of experimental conditions

To fulfill the ultrasensitive detection of NT-proBNP, the influence of experimental conditions including the amount of $Mn(CH_3COO)_2$, the pH of phosphate buffer saline, the concentration of $K_2S_2O_8$ and the incubation time of Ab_2 bioconjugate on the ECL response were

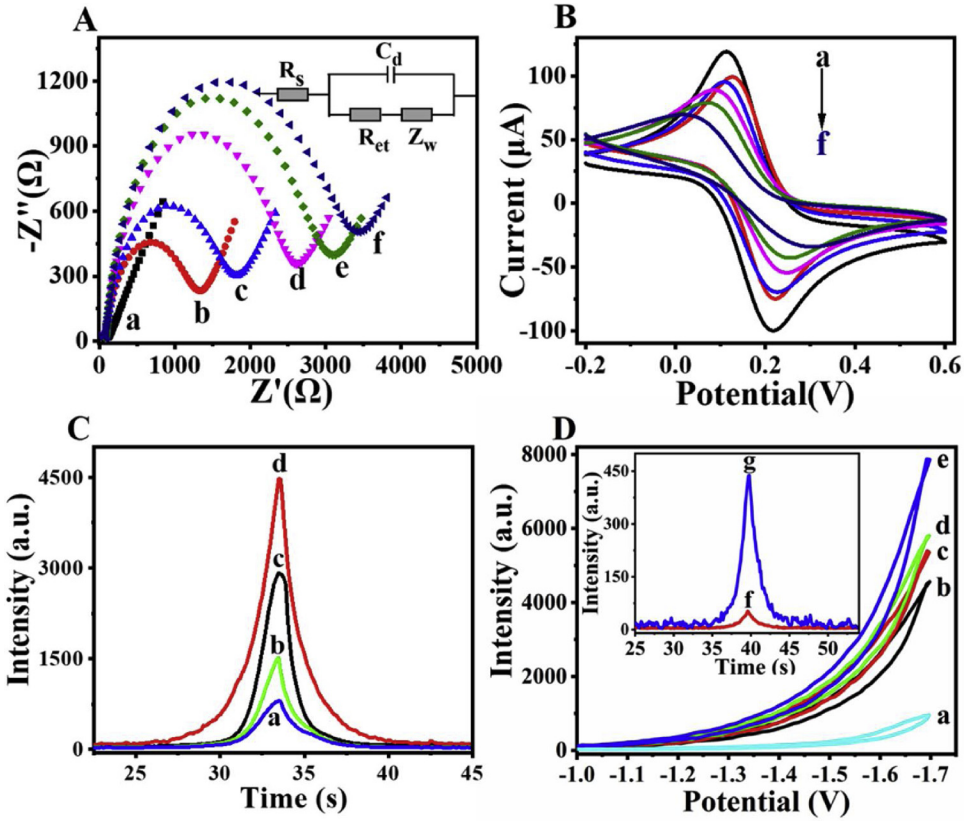

Fig. 3. (A) EIS and (B) CV curves of GCE (a), MoS_2@Cu_2S-Au/GCE (b), Ab_1/MoS_2@Cu_2S-Au/GCE (c), immunosensor (d), Ag/immunosensor (e), MZnAgInS/ZnS@t-UiO-66-NH_2-Ab_2/Ag/immunosensor (f). Inset in A: equivalent circuit for EIS. (C) ECL intensity of ZnAgInS (a), MZnAgInS (b), MZnAgInS/ZnS (c) and MZnAgInS/ZnS@t-UiO-66-NH_2 (d) modified GCE in 10 mL of PBS (pH 7.5) containing 0.1 M $K_2S_2O_8$. (D) ECL intensity-potential curves of MZnAgInS/ZnS@t-UiO-66-NH_2/GCE in 10 mL of PBS (pH 7.5) (a), and 10 mL of PBS (pH 7.5) containing 0.1 M $K_2S_2O_8$ (b), 0.1 M $K_2S_2O_8$ and 500 μL of 1 mg mL^{-1} Cu_2S (c), MoS_2 (d) and MoS_2@Cu_2S (e). Inset in D: ECL intensity of GCE in 10 mL of PBS (pH 7.5) containing 0.1 M $K_2S_2O_8$ (f) and PBS (pH 7.5) containing 0.1 M $K_2S_2O_8$ and 500 μL of 1 mg mL^{-1} MoS_2@Cu_2S (g).

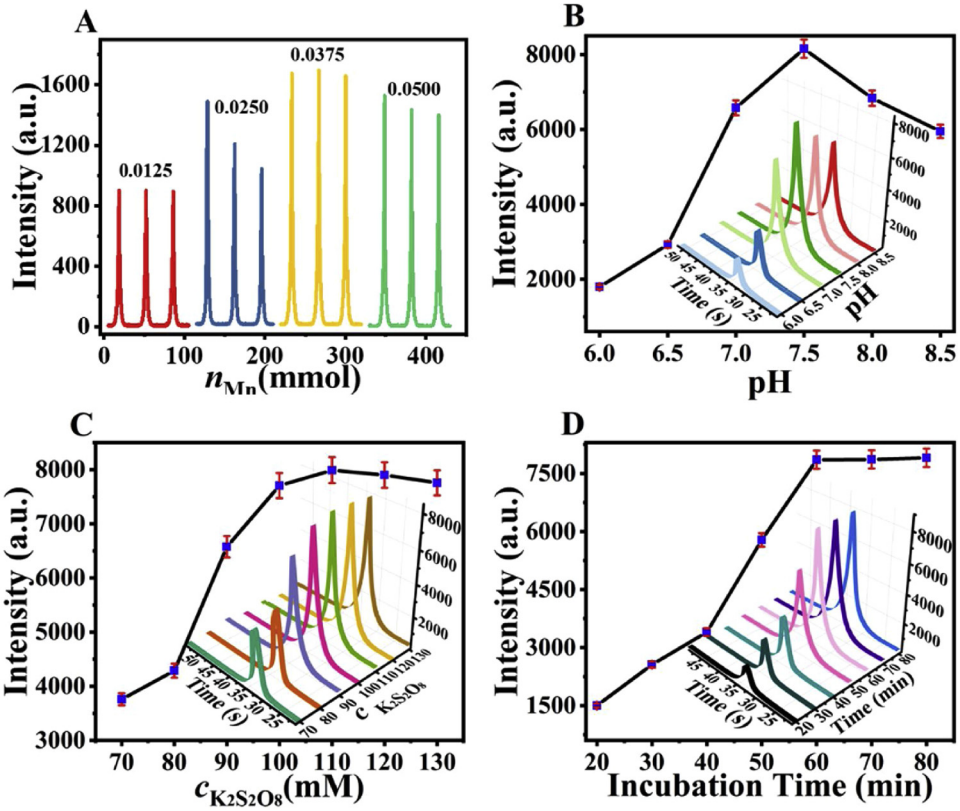

Fig. 4. Optimization of (A) the amount of $Mn(CH_3COO)_2$, (B) pH of PBS, (C) concentration of $K_2S_2O_8$ and (D) incubation time of Ab_2 bioconjugate.

examined. In view of the fact that the complex environment of Mn coordinated in multinary MZnAgInS NCs may influence the emission energy and optical property of MznAgInS [34], we investigated the effect of Mn doping level on the ECL performance of MZnAgInS NC by adding different amounts of $Mn(CH_3COO)_2$ during the preparation of MZnAgInS. As shown in Fig. 4A, the ECL intensities of MZnAgInS with 0.0125 or 0.0250 mmol Mn dopant were either low or fluctuant, while MZnAgInS with 0.0375 mmol Mn dopant possessed the desirable ECL response. Once the Mn dopant amount increased to 0.0500 mmol, the ECL intensity decreased again probably due to more Mn dopants in host NCs could cause more lattice strain to decline the quantum yield [35]. Hence, 0.0375 mmol was chosen as the appropriate Mn doping amount. Meanwhile, to inspect the effect of pH exerted on the ECL response, PBS with pH ranging from 6.0–8.5 was tested. As seen from Fig. 4B, for better bioactivity of biomolecules as well as stronger ECL intensity of immunosensor, pH 7.5 was accepted in the ensuing work. Besides, the concentration of coreactant was optimized to achieve better ECL performance (Fig. 4C). As the concentration of $K_2S_2O_8$ increased from 70 mM to 110 mM, more MZnAgInS/ZnS excited states are generated from the oxidation of MZnAgInS/$ZnS^{\cdot -}$ by the electrogenerated radical $SO4^{\cdot -}$. When the $K_2S_2O_8$ concentration exceeded 110 mM, the ECL intensity decreased for the reason that excess $S_2O_8^{2-}$ reacted directly with MZnAgInS/$ZnS^{\cdot -}$ thus restrained the formation of MZnAgInS/ZnS excited state. Therefore, the following experiments used 110 mM of $K_2S_2O_8$ as the coreactant. The incubation time of Ab_2 bioconjugate was also optimized to be 60 min (Fig. 4D).

3.5. Analytical performance of ECL immunosensor

Under optimal experimental conditions, the ECL intensity increased with the rising concentration of NT-proBNP from 1 fg mL^{-1} to 100 ng mL^{-1} (Fig. 5A), which showed a linear plot with the equation of $I = 7817.4 + 924.3 \lg c$ (in which I represents the ECL intensity and c is the NT-proBNP concentration, pg mL^{-1}) (Fig. 5B). Based on the definition of limit of detection (LOD) prescribed by IUPAC [36], the LOD was determined to be 0.41 fg mL^{-1} (Fig. S2). The comparison for existing NT-proBNP bioassays were listed in Table S2, from which our protocol was found to possess the highest sensitivity and widest detection range thanks to the excellent conductivity and catalytic property of MoS_2@Cu_2S-Au as well as the unrivalled ECL capacity of MZnAgInS/ZnS NC.

Selectivity was also recognized as a paramount assessment for practical potential of ECL immunosensor, thus cardiactroponinI (cTnI), cardiactroponinT (cTnT), human serum albumin (HSA) and C-reactive protein (CRP) were chosen as possible interfering proteins to test the selectivity of this immunosensor. As shown in Fig. 5C, the presence of interferences with higher concentration (100 pg mL^{-1}) than target NT-proBNP (1 pg mL^{-1}) exerted neglectable influence on the ECL intensity, demonstrating the desirable selectivity of this immunosensor towards NT-proBNP. The stability of the immunosensor, including operational stability and long-term storage stability, were also examined and displayed in Fig. 5D and E, respectively. As consecutive cyclic scanning to various concentrations of NT-proBNP, the ECL responses exhibited little fluctuation, manifesting the satisfying operation stability of this strategy. The long-term storage stability was tested by storing this immunosensor in refrigerator. After the storage of 5, 10, 15 and 20 days, the ECL intensity turned to be 94.0 %, 89.3 %, 85.2 % and 81.5 % of its initial value, respectively. Therefore, this immunosensor exhibited excellent stability. The reproducibility of this ECL immunosensor was determined by measuring the same NT-proBNP concentration (1 pg mL^{-1}) using six immunosensors prepared in a same batch and one immunosensor prepared in six different batches, which showed the relative standard deviation (RSD) of less than 5 % (Fig. 5F), indicating the acceptable reproducibility of this immunosensor.

3.6. Analysis of NT-proBNP in real samples

To validate the potential of this ECL immunosensor in clinical

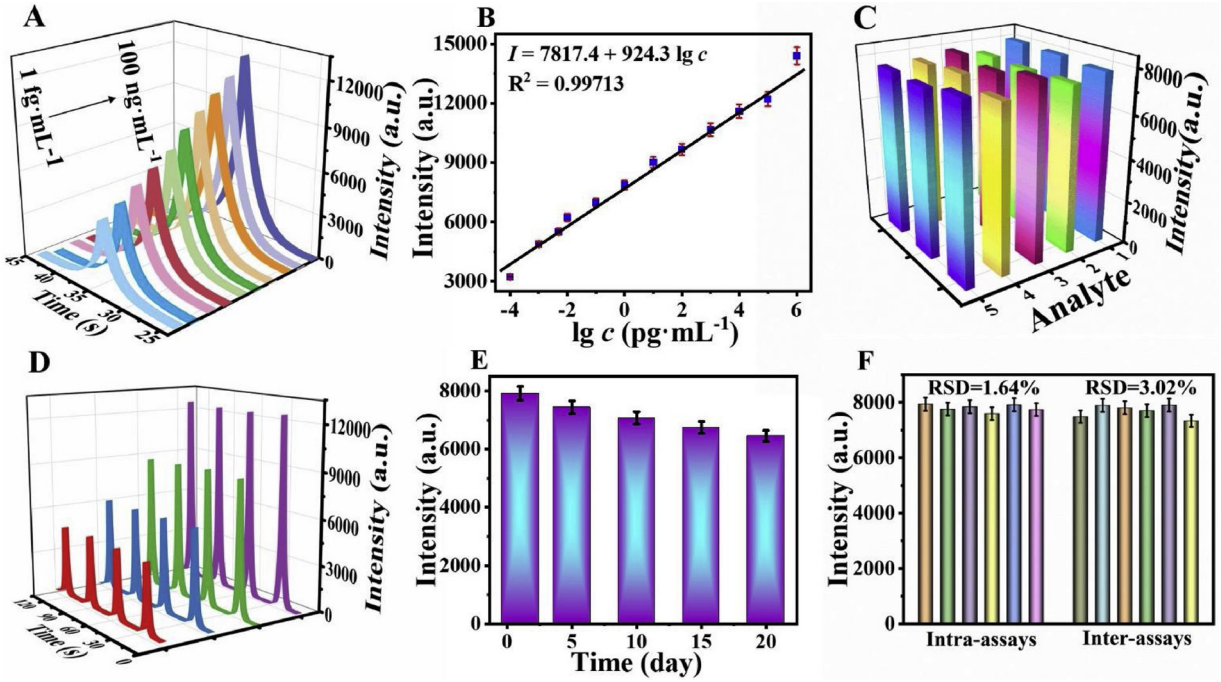

Fig. 5. (A) ECL intensity-time curves of the immunosensor in the presence of 0.001, 0.005, 0.01, 0.1, 0.5, 1, 10, 100, 1000, 10,000 and 100,000 pg mL^{-1} NT-proBNP. (B) Calibration plot of the immunosensor. (C) Selectivity of the immunosensor for 1 pg mL^{-1} of NT-proBNP (1), and the mixture of 1 pg mL^{-1} of NT-proBNP and 100 pg mL^{-1} of cTnI (2), cTnT (3), HSA (4) and CRP (5). (D) Stability of the immunosensor to 0.001 (a), 0.01 (b), 10 (c) and 100 (d) pg mL^{-1} NT-proBNP. (E) Long-term storage stability of the immunosensor for detection of 1 pg mL^{-1} of NT-proBNP. (F) Reproducibility of the immunosensor for detection of 1 pg mL^{-1} of NT-proBNP. (Error bar = SD, n = 5).

Table 1
NT-proBNP detection in human serum samples.

Serum sample content (pg mL^{-1})	Added (pg mL^{-1})	Found (pg mL^{-1})	Average value (pg mL^{-1})	RSD (%)	Recovery (%)
0.019	0.010	0.027, 0.032, 0.029, 0.028, 0.031	0.0294	7.1	104
	0.020	0.035, 0.038, 0.040, 0.039, 0.042	0.0388	6.7	99
	0.050	0.064, 0.067, 0.072, 0.068, 0.070	0.0682	4.4	98.4
27.4	10	39.3, 35.4, 37.2, 34.7, 40.1	37.3	6.3	99.4
	20	49.5, 45.2, 47.3, 46.8, 50.4	47.8	4.4	102.2
	50	76.4, 73.3, 78.6, 80.3, 77.8	77.3	3.4	99.7
32,800	20,000	50,200, 54,600, 51,800, 49,100, 55,300	52,200	5.2	97.0
	30,000	59,700, 61,300, 65,100, 60,800, 63,600	62,100	3.5	97.7
	50,000	80,900, 84,600, 79,500, 83,100, 82,200	82,200	2.4	98.8

application for NT-proBNP detection, we conducted the recovery experiment in human serum sample based on standard addition method. Prior to analysis, human serum sample was diluted 5 folds with PBS. The average NT-proBNP content of three sample were calculated to be 19.0 fg mL^{-1}, 27.4 pg mL^{-1} and 32.8 ng mL^{-1} after testing the samples five times, respectively. Next, proper amount standard solution of NT-proBNP (denoted as Added) were added in the serum samples and the correlative NT-proBNP concentration (denoted as Found) were obtained after the ECL intensity tested 5 times. The RSD, which was listed in Table 1, was figured to be less than 7 % with acceptable recoveries ranged from 99.4%–102.2%, proving that the proposed immunoassay hold infinite application prospect in clinical accessment of NT-proBNP. Furthermore, the precision of our immunosensor was challenged with traditional enzyme-linked immunosorbent assay (ELISA) kit via F-test and t-test. As depicted in Table S3, the calculated F value and t value were far below the theoretical ones, proving that the significant difference between the two methods was negligible.

4. Conclusion

This work constructs a novel ECL system for ultrasensitive immunosensing of NT-proBNP by using MZnAgInS/ZnS@t-UiO-66-NH_2 as the luminophore and MoS_2@Cu_2S as the coreaction accelerator. Such an ultrasensitive ECL biosensor presents the following glamorous properties. Essentially, the ECL behavior of MZnAgInS/ZnS is applied in immunosensing for the first time. Appropriate Mn doping enhances the stable luminescence, and the presence of ZnS shell reduces the surface defects to boost the quantum yield. Additionally, considering the small size distribution of MZnAgInS/ZnS NCs, thermally-treated UiO-66-NH_2 with enlarged pore diameter is functioned as anchor carrier to load more luminophores for signal amplification. Moreover, to achieve high ECL efficiency, snowflake-like MoS_2@Cu_2S composite with considerable catalytic active sites is synthesized as coreaction accelerator of $K_2S_2O_8$ reduction. The proposed ECL immunosensor realizes the ultrasensitive quantification of NT-proBNP from 1 fg mL^{-1} to 100 ng mL^{-1}, and the detection limit is down to 0.41 fg mL^{-1}. Given the high selectivity, good stability, excellent reproducibility, and acceptable recovery for practical application, the elaborated ECL immunosensor would inspire more interest in MOFs-based luminophore and light up an innovative avenue for biomarkers analysis.

Declaration of Competing Interest

The authors declare that they have no known competing financial

interests or personal relationships that could have appeared to influence the work reported in this paper

Acknowledgements

This study was supported by the National Key Scientific Instrument and Equipment Development Project of China (No. 21627809), National Natural Science Foundation of China (Nos. 21505051, 21575050, 21607055, 21777056), Jinan Scientific Research Leader Workshop Project (2018GXRC024). Ju thanks the Special Foundation for Taishan Scholar Professorship of Shandong Province (No. ts201712052) and UJN.

Appendix A. Supplementary data

Supplementary material related to this article can be found, in the online version, at doi:https://doi.org/10.1016/j.snb.2019.127619.

References

[1] K. Dworzynski, E. Roberts, A. Ludman, J. Mant, Diagnosing and managing acute heart failure in adults: summary of NICE guidance, BMJ 349 (2014) 5695–5698.
[2] W. Thomas, A. Johann, E. Bernd, The diagnostic and prognostic value of brain natriuretic peptide and aminoterminal-pro brain natriuretic peptide, Curr. Pharm. Des. 11 (2005) 511–525.
[3] X. Liu, Y. Huang, M. Lai, J. Chen, T. Chu, P.K. Tasy, et al., Predicting cardiogenic pulmonary edema in heart failure patients by using an N-terminal Pro-b-type natriuretic peptide (NT-pro BNP)-Based score, Clin. Chim. Acta 480 (2018) 26–33.
[4] Y. He, Y. Wang, X. Yang, S. Xie, R. Yuan, Y. Chai, Metal organic frameworks combining $CoFe_2O_4$ magnetic nanoparticles as highly efficient SERS sensing platform for ultrasensitive detection of N-Terminal pro-brain natriuretic peptide, ACS Appl. Mater. Interface 8 (2016) 7683–7690.
[5] Y. Zhuo, W. Yi, W. Liang, R. Yuan, Y. Chai, A. Chen, et al., Ultrasensitive electrochemical strategy for NT-proBNP detection with gold nanochains and horseradish peroxidase complex amplification, Biosens. Bioelectron. 26 (2011) 2188–2193.
[6] T. Nishikimi, H. Okamoto, M. Nakamura, N. Ogawa, K. Horii, K. Nagata, et al., Direct immunochemiluminescent assay for Pro-BNP and total BNP in human plasma-ProBNP and total BNP levels in healthy individuals and heart failure patients, PLoS One 8 (2013) 53233–53241.
[7] Y. Qian, J. Feng, D. Fan, Y. Zhang, X. Kuang, H. Wang, et al., A sandwich-type photoelectrochemical immunosensor for NT-pro BNP detection based on F-Bi_2WO_6/Ag_2S and GO/PDA for signal amplification, Biosens. Bioelectron. 131 (2019) 299–306.
[8] N. Wang, Y. Feng, Y. Wang, H. Ju, F. Yan, Electrochemiluminescent imaging for multi-immunoassay sensitized by dual DNA amplification of polymer dot signal, Anal. Chem. 90 (2018) 7708–7714.
[9] L. Li, Y. Chen, J. Zhu, Recent advances in electrochemiluminescence analysis, Anal. Chem. 89 (2017) 358–371.
[10] G. Zou, H. Ju, Electrogenerated chemiluminescence from a CdSe nanocrystal film and its sensing application in aqueous solution, Anal. Chem. 76 (2004) 6871–6876.
[11] X. Liu, H. Jiang, J. Lei, H. Ju, Anodic electrochemiluminescence of CdTe quantum dots and its energy transfer for detection of catechol derivatives, Anal. Chem. 79 (2007) 8055–8060.
[12] L. Cheng, X. Liu, J. Lei, H. Ju, Low-potential electrochemiluminescent sensing based on surface unpassivation of CdTe quantum dots and competition of analyte cation to stabilizer, Anal. Chem. 82 (2010) 3359–3364.
[13] Y. Sun, X. Wu, K. Zhang, Q. Ren, R. Xie, Electrochemiluminescent quaternary Cu-Zn-In-S nanocrystals as a sensing platform: enzyme-free and sensitive detection of the FLT3 gene based on triple signal amplification, Biosens. Bioelectron. 100 (2018) 445–452.
[14] B. Zhang, F. Zhang, P. Zhang, D. Shen, X. Gao, G. Zou, Ultrasensitive electrochemiluminescent sensor for MicroRNA with multinary Zn-Ag-In-S/ZnS nanocrystals as tags, Anal. Chem. 91 (2019) 3754–3758.
[15] M. Ko, H.C. Yoon, H. Yoo, H.O. Ji, H. Yang, Y.R. Do, Highly efficient green Zn-Ag-In-S/Zn-In-S/ZnS QDs by a strong exothermic reaction for down-converted green and tripackage white LEDs, Adv. Funct. Mater. 27 (2017) 1602638–1602647.
[16] R.N. Bhargava, D. Gallagher, X. Hong, A. Nurmikko, Optical properties of manganese-doped nanocrystals of ZnS, Phys. Rev. Lett. 72 (1994) 416–419.
[17] G. Manna, S. Jana, R. Bose, N. Pradhan, Mn-doped multinary CIZS and AIZS nanocrystals, J. Phys. Chem. Lett. 3 (2012) 2528–2534.
[18] Y. Shan, J. Xu, H. Chen, Enhanced electrochemiluminescence quenching of CdS:Mn nanocrystals by CdTe QDs-Doped silica nanoparticles for ultrasensitive detection of thrombin, Nanoscale 3 (2011) 2916–2923.
[19] X. Tang, Z. Zu, L. Bian, J. Du, W. Chen, X. Zeng, et al., Synthesis of Mn doping Ag-In-Zn-S nanoparticles and their photoluminescence properties, Mater. Des. 91 (2016) 256–261.
[20] Y. Chen, S. Li, L. Huang, D. Pan, Green and facile synthesis of water-soluble Cu-In-S/ZnS core/shell quantum dots, Inorg. Chem. 52 (2013) 7819–7821.
[21] Z. Wang, Z. Yan, F. Wang, J. Cai, L. Guo, J. Su, et al., Highly sensitive photoelectrochemical biosensor for kinase activity detection and inhibition based on the surface defect recognition and multiple signal amplification of metal-organic frameworks, Biosens. Bioelectron. 97 (2017) 107–114.
[22] M. Pourkhosravani, S. Dehghanpour, F. Farzaneh, Palladium nanoparticles supported on zirconium metal organic framework as an efficient heterogeneous catalyst for the suzuki-miyaura coupling reaction, Catal. Lett. 146 (2016) 499–508.
[23] S. Chen, L. Zhang, Z. Zhang, G. Qian, Z. Liu, Q. Cui, et al., Study on the desorption process of n-Heptane and methyl cyclohexane using UiO-66 with hierarchical pores, ACS Appl. Mater. Interface 10 (2018) 21612–21618.
[24] R. Zhang, B. Du, Q. Li, Z. Cao, G. Feng, X. Wang, α-Fe_2O_3 nanoclusters confined into UiO-66 for efficient visible-light photodegradation performance, Appl. Surf. Sci. 466 (2019) 956–963.
[25] F.F. Wu, Y. Zhou, H. Zhang, R. Yuan, Y.Q. Chai, Electrochemiluminescence peptide-based biosensor with Hetero-Nanostructures as coreaction accelerator for the ultrasensitive determination of tryptase, Anal. Chem. (2018) 2263–2270.
[26] Y. Zhou, S. Chen, X. Luo, Y. Chai, R. Yuan, Ternary electrochemiluminescence nanostructure of Au nanoclusters as a highly efficient signal label for ultrasensitive detection of cancer biomarkers, Anal. Chem. 90 (2018) 10024–10030.
[27] S. Li, Z. Liu, J. Li, A. Chen, Z. Ying, Enzyme-free target recycling and double-output amplification system for electrochemiluminescent assay of mucin 1 with MoS_2 nanoflowers as Co-reaction accelerator, ACS Appl. Mater. Interface 10 (2018) 14483–14490.
[28] X. Song, X. Li, D. Wei, R. Feng, T. Yan, Y. Wang, et al., CuS as Co-reaction accelerator in PTCA-$K_2S_2O_8$ system for enhancing electrochemiluminescence behavior of PTCA and its application in detection of amyloid-β protein, Biosens. Bioelectron. 126 (2019) 222–229.
[29] Z. Liu, S. Li, R. Wei, A. Chen, Y. Chai, R. Yuan, et al., CuS porous nanospheres as a novel noble metal-free Co-reaction accelerator for enhancing electrochemiluminescence and sensitive immunoassay of mucin 1, Sens. Actuators B: Chem. 274 (2018) 110–115.
[30] X. Zhang, Y. Guo, T. Jian, B. Sun, Z. Liang, X. Xu, et al., Controllable growth of MoS_2 nanosheets on novel Cu_2S snowflakes with high photocatalytic activity, Appl. Catal. B: Environ. 232 (2018) 355–364.
[31] Z. Yan, F. Wang, P. Deng, Y. Wang, K. Cai, Y. Chen, et al., Sensitive electrogenerated chemiluminescence biosensors for protein kinase activity analysis based on bimetallic catalysis signal amplification and recognition of Au and Pt loaded metal-organic frameworks nanocomposites, Biosens. Bioelectron. 109 (2018) 132–138.
[32] M.S. Zaeimian, B. Gallian, C. Harrison, W. Yu, J. Zhao, X. Zhu, Mn doped AZIS/ZnS nanocrystals (NCs): effects of Ag and Mn levels on NC optical properties, J. Alloys Compd. 765 (2018) 236–244.
[33] X. Long, F. Zhang, Y. He, S. Hou, B. Zhang, G. Zou, The promising anodic electrochemiluminescence of non-toxic and core/shell $CuInS_2$/ZnS NCs in aqueous medium and its bio-sensing potential, Anal. Chem. 90 (2018) 3563–3569.
[34] J. Zhu, S. Mei, W. Yang, G. Zhang, Q. Chen, W. Zhang, et al., Tunable emission of Cu (Mn)-doped ZnInS quantum dots via dopant interaction, J. Colloid Interface Sci. 506 (2017) 27–35.
[35] S. Chen, M.S. Zaeimian, J.H.S.K. Monteiro, J. Zhao, A.G. Mamalis, A.D. Bettencourt-Dias, et al., Mn doped AIZS/ZnS nanocrystals: synthesis and optical properties, J. Alloys Compd. 725 (2017) 1077–1083.
[36] G.L. Long, J.D. Winefordner, Limit of detection: a closer look at the IUPAC definition, Anal. Chem. 55 (1983) 712–724.

Chao Wang studies in school of chemistry and chemical engineering, University of Jinan as a postgraduate student. She is working on designing electrochemiluminescence sensors.

Lei Liu received the Ph.D. degree from China University of Geosciences (Beijing), Beijing, China. She is a post-doctoral of school of chemistry and chemical engineering at University of Jinan, Shandong, China. Her research interests focus on the construction of nanomaterials for fuel cell and biosensors with diseases, energy and environment applications.

Xuejing Liu received her Ph.D. degree in College of Chemistry from Dalian University of Technology in 2015. From 2015 to 2018, she worked as a postdoctoral fellow in Dalian Institute of Chemical Physics. At present, she begins to work in School of Chemistry and Chemical Engineering from University of Jinan. Her main interest is in the theoretical investigation of catalyst materials for applications in small molecules activation and conversion, electrocatalytic of water splitting, reduction of CO_2 and N_2, etc.

Yu Chen studies in school of chemistry and chemical engineering, University of Jinan as a junior student. She is working on designing electrochemiluminescence sensors and nanomaterials.

Xueying Wang received her Ph.D. in analytical chemistry from Wuhan University. She is now working as a lectorate in School of Chemistry and Chemical Engineering in University of Jinan. She has been hosting two of national and provincial scientific research projects. Currently, her research interests focus on the design and fabrication of microfluidic device for the synthesis of nanomaterials and her other research activities include constructing 3D vascular network for the engineering of three-dimensional cell culture microenvironment in vitro.

Dawei Fan received her Ph. D degree from Lanzhou institute of chemical physics, Chinese academy of sciences. Now, she is an associate professor at University of Jinan. Her main research interests are electrochemical sensors and photoelectrochemical sensors. She has published over 50 articles on analysis, immunosensor and applied successfully for many

research projects, such as Angewandte Chemie International Edition, Biosensors & Bioelectronics, Journal of Physical Chemistry C, and ACS Applied Materials & Interfaces.

Xuan Kuang obtained her Ph.D. in Analytical Chemistry in 2015. Her research interests focus on metal organic materials and the application of nanomaterials to electrochemical sensors, synthesis and fundamental electrochemical studies of energy storage devices and synthetic nanomotors.

Xu Sun received her Ph.D. in inorganic chemistry at University of Science and Technology of China (USTC). She is now working as an associate professor in School of Chemistry and Chemical Engineering in University of Jinan. Currently, her research interests focus on the design and fabrication of novel nanomaterials for the construction of energy-related devices.

Qin Wei, a professor and DSc, has devoted herself to analytical teaching and scientific research. Her main research interests are the determination of protein and nucleic acid by photometry and the electrochemical immunosensor preparation. She has published over one hundred articles on analysis, immunosensor and applied successfully for many research projects, such as *Biomaterials, Adv. Funct. Mater., Biosens. Bioelectron., Sens. Actuators B: Chem., Talanta.*

Huangxian Ju received his BS, MS and Ph.D. degrees from Nanjing University during 1982-1992. He was a postdoc in Montreal University (Canada) from 1996 to 1997 and a guest professor in three universities of Germany and Ireland in 1999–2000. He became an associate and full professor of Nanjing University in 1993 and 1999. He is currently the director of State Key Laboratory of Analytical Chemistry for Life Science. His research interests focus on analytical biochemistry, biosensing and molecular diagnosis. He has published 616 papers in different journals with SCI h-index of 83 (29,523 citations) and Google Scholar h-index of 91 with more than 29,000 citations.